Published in final edited form as:
Free Radic Biol Med. 2017 January ; 102: 248–259. doi:10.1016/j.freeradbiomed.2016.11.049.

Intact mitochondrial Ca^{2+} uniport is essential for agonist-induced activation of endothelial nitric oxide synthase (eNOS)

Suphachai Charoensin[a], **Emrah Eroglu**[a], **Marissa Opelt**[b], **Helmut Bischof**[a], **Corina T. Madreiter-Sokolowski**[a], **Andrijana Kirsch**[a], **Maria R. Depaoli**[a], **Saša Frank**[a], **Astrid Schrammel**[b], **Bernd Mayer**[b], **Markus Waldeck-Weiermair**[a], **Wolfgang F. Graier**[a], and **Roland Malli**[a,*]

[a]Institute of Molecular Biology and Biochemistry, Center of Molecular Medicine, Medical University of Graz, Austria

[b]Institute of Pharmaceutical Sciences, Department of Pharmacology and Toxicology, University of Graz, Austria

Abstract

Mitochondrial Ca^{2+} uptake regulates diverse endothelial cell functions and has also been related to nitric oxide ($NO^{\bullet}$) production. However, it is not entirely clear if the organelles support or counteract $NO^{\bullet}$ biosynthesis by taking up Ca^{2+}. The objective of this study was to verify whether or not mitochondrial Ca^{2+} uptake influences Ca^{2+}-triggered $NO^{\bullet}$ generation by endothelial $NO^{\bullet}$ synthase (eNOS) in an immortalized endothelial cell line (EA.hy926), respective primary human umbilical vein endothelial cells (HUVECs) and eNOS-RFP (red fluorescent protein) expressing human embryonic kidney (HEK293) cells. We used novel genetically encoded fluorescent $NO^{\bullet}$ probes, the geNOps, and Ca^{2+} sensors to monitor single cell $NO^{\bullet}$ and Ca^{2+} dynamics upon cell treatment with ATP, an inositol 1,4,5-trisphosphate (IP_3)-generating agonist. Mitochondrial Ca^{2+} uptake was specifically manipulated by siRNA-mediated knock-down of recently identified key components of the mitochondrial Ca^{2+} uniporter machinery. In endothelial cells and the eNOS-RFP expressing HEK293 cells we show that reduced mitochondrial Ca^{2+} uptake upon the knock-down of the mitochondrial calcium uniporter (MCU) protein and the essential MCU regulator (EMRE) yield considerable attenuation of the Ca^{2+}-triggered $NO^{\bullet}$ increase independently of global cytosolic Ca^{2+} signals. The knock-down of mitochondrial calcium uptake 1 (MICU1), a gatekeeper of the MCU, increased both mitochondrial Ca^{2+} sequestration and Ca^{2+}-induced $NO^{\bullet}$ signals. The positive correlation between mitochondrial Ca^{2+} elevation and $NO^{\bullet}$ production was independent of eNOS phosphorylation at $serine^{1177}$. Our findings emphasize that manipulating mitochondrial Ca^{2+} uptake may represent a novel strategy to control eNOS-mediated $NO^{\bullet}$ production.

*Correspondence to: Institute of Molecular Biology and Biochemistry, Research Unit for Molecular and Cellular Physiology, Center of Molecular Medicine, Medical University of Graz, Harrachgasse 21/III, Graz, Austria. roland.malli@medunigraz.at (R. Malli).

Disclosures
None.

Europe PMC Funders Author Manuscripts

Keywords

Calcium; Endothelial nitric oxide production; ENOS; GeNOps; Mitochondria

1 Introduction

The transfer of Ca^{2+} into mitochondria influences cell signaling and functions by various means. The organelles themselves immediately respond to Ca^{2+} elevations as they house Ca^{2+}-sensitive enzymes and transporters [1]. Ca^{2+} within mitochondria is known to elevate their metabolic activity, but can also trigger cell death [2,3]. In addition, mitochondrial Ca^{2+} uptake and release shapes local and global cellular Ca^{2+} signals, which control a variety of cell signaling events [4]. Particularly, in vascular endothelial cells mitochondrial Ca^{2+} signals have been debated to directly or indirectly control key functions such as the synthesis and release of vasoactive compounds [5,6]. However, the exact role of mitochondrial Ca^{2+} uptake for endothelial nitric oxide ($NO^{\bullet}$) production, which is accomplished predominately by the Ca^{2+} calmodulin-dependent endothelial nitric oxide synthase (eNOS) [7], is unknown. While mitochondria-derived $NO^{\bullet}$ has been detected in isolated mitochondria and permeabilized endothelial cells [5,8], the impact of mitochondrial Ca^{2+} uptake on Ca^{2+}-evoked $NO^{\bullet}$ production in intact cells has not been investigated so far.

In recent years the key components of mitochondrial Ca^{2+} channels have been identified [9,10]. These studies unveiled that the mitochondrial Ca^{2+} uniporter basically consists of the pore forming mitochondrial calcium uniporter (MCU) [9], the essential MCU regulator (EMRE) [11], and the mitochondrial calcium uptake 1 (MICU1) [10]. Interestingly, MICU1 shields the MCU/EMRE-dependent mitochondrial Ca^{2+} channel and thereby impedes mitochondrial Ca^{2+} uptake under basal conditions [11]. A very recent study unveiled that MICU1 methylation by protein arginine methyltransferase-1 (PRMT1) hampers MCU activation by Ca^{2+}, indicating that mitochondrial Ca^{2+} uptake is tightly controlled by posttranslational modifications [12]. However, the knock-down of these key components of the mitochondrial Ca^{2+} uniporter allows to efficiently manipulate mitochondrial Ca^{2+} uptake [13]. Based on these findings the role of mitochondrial Ca^{2+} uptake for endothelial $NO^{\bullet}$ production in intact cells has not been reinvestigated so far. Here we used novel genetically encoded fluorescent $NO^{\bullet}$ probes, the geNOps, to monitor $NO^{\bullet}$ signals on the level of individual cells. Recently, geNOps were used to specifically visualize the biotransformation of nitroglycerine to $NO^{\bullet}$ by aldehyde dehydrogenase-2 (ALDH2) in single vascular smooth muscle cells [14]. Herein we combined the geNOp technology with Ca^{2+} sensors and siRNA-mediated knock-down of mitochondrial Ca^{2+} channel proteins [15]. This approach allowed us to demonstrate that Ca^{2+}-triggered $NO^{\bullet}$ production by eNOS is positively controlled by mitochondrial Ca^{2+} uniport independently of global cytosolic Ca^{2+} signals. Hence, this study unveiled a clear link between mitochondrial Ca^{2+} uptake and eNOS-mediated $NO^{\bullet}$ generation which might have several implications in health and diseases.

Europe PMC Funders Author Manuscripts

2 Materials and methods

2.1 Chemicals

Dulbecco's modified Eagle's medium (DMEM), antimycin, oligomycin, and L-N^G-nitro arginine were purchased from Sigma-Aldrich (Vienna, Austria). Fura-2-acetoxymethyl ester (fura-2/am), tetramethylrhodamine methyl ester perchlorate (TMRM) and cell culture supplements were obtained from Invitrogen (San Diego, USA). TransFast™ transfection reagent was obtained from Promega (Mannheim, Germany). Antibodies against total and phosphorylated eNOS (pS1177) were from BD Transduction Laboratories™, alpha-tubulin was from Cell Signaling Technology®. Adenosine-5´-triphosphate (ATP) and all other chemicals were purchased from Roth (Karlsruhe, Germany) unless otherwise indicated.

2.2 Cell culture, transfection and adenoviral transduction

The human umbilical vein endothelial cell line EA.hy92 (passage 35–45) [16] was cultured in DMEM medium containing 1% HAT (5 mM hypoxanthine, 20 μM aminopterin, 0.8 mM thymidine), 10% fetal bovine serum, 100 U/ml penicillin, and 100 μg/ml streptomycin in a humidified incubator (37 °C, 5% CO_2). Human embryonic kidney cells HEK293 were grown in a culture medium without HAT. Prior to transfection or adenoviral transduction cells were plated on 30 mm glass cover slips. At 50–60% confluence, cells were co-transfected with 100 μM of the respective siRNA(s) and 1.5 μg of a plasmid coding either for the $NO^•$-sensitive probe G-geNOp, its mutated $NO^•$-insensitive negative control (G-geNOp^{mut}) (NGFI Next Generation Fluorescence Imaging GmbH, Graz, Austria), the mitochondrial cameleon 4mtD3cpv or the endothelial nitric oxide synthase C-terminally fused to a red fluorescent protein (eNOS-RFP) as described previously [13]. All siRNAs were purchased from Microsynth (Balgach, Switzerland) and their (5´–3´) sequences were: GCAGCUCAAGAAGCACUUCAA (hMICU1-si1), GCAAUGGCGAACUGAGCAAUA (hMICU1-si2), AGAAGUCUGUGAUGAUAAA (hMICU1-si3), GCCAGAGACAGACAAUACU (hMCU-si1), GGAAAGGGAGCUUAUUGAA (hMCU-si2), GAACUUUGCUGCUCUACUU (hEMRE-si) and a scrambled negative control siRNA UUCUCCGAACGUGUCACGU (Scrambled siRNA). Human umbilical vein endothelial cells (HUVECs) (CC-2519; Lonza, Basel, Switzerland) were grown at 37 °C and 5% CO_2 on tissue culture dishes coated with 1% Gelatin (#49391; Sigma) in endothelial basal medium (EBM) culture medium (CC-3121; Lonza) supplemented with endothelial growth medium (EGM) SingleQuots and growth factors (CC-4143; Lonza). HUVECs were cultured maximally 14 days before experiments. For imaging experiments HUVECs were seeded on 1% Gelatin coated 30 mm glass cover slips. At a confluence of 50–60% siRNA transfections and infection of BacMam 4mtD3cpv virus (Life Technologies, Vienna, Austria) encoding the mitochondrial cameleon was performed as recently described [12]. The G-geNOp expression in endothelial cells was achieved by adenoviral transduction at a multiplicity of infection (MOI) of 10 for HUVECs or MOI 1000 for EA.hy926 cells. All experiments were performed 42–54 h after transfection or infection, respectively.

2.3 Buffer solutions for imaging experiments

For imaging of cytosolic Ca^{2+} or mitochondrial membrane potential, cells were loaded at room temperature with either 3.3 μM fura2/am or 100 nM TMRM, respectively

supplemented in a storage buffer composed of 138 mM NaCl, 2 mM $CaCl_2$, 5 mM KCl, 1 mM $MgCl_2$, 1 mM HEPES, 2.6 mM $NaHCO_3$, 0.44 mM KH_2PO_4, 0.34 mM Na_2HPO_4, 10 mM D-glucose, 0.1% vitamins, 0.2% essential amino acids, and 1% penicillin/streptomycin, pH 7.4 for 40 min. Prior to $NO^{\bullet}$ measurements G-geNOp-expressing EA.hy926 cells were incubated at room temperature in a ferrous fumarate/ascorbic acid buffer for 20 min and maintained in storage buffer for at least 1 h. For dual recordings of $NO^{\bullet}$ and cytosolic Ca^{2+}, Fura2/am loading was done after ferrous fumarate incubation as recently described [15]. All imaging experiments were performed by perfusing cells in a HEPES-buffered solution (HBS) containing 138 mM NaCl, 5 mM KCl, 2 mM $CaCl_2$, 1 $MgCl_2$, 10 mM D-glucose, 10 mM HEPES, pH 7.4. For Ca^{2+}-free conditions HBS containing 1 mM EGTA instead of $CaCl_2$ was used.

2.4 Fluorescence microscopy

For fluorescent recordings an advanced wide-field fluorescent microscope (Till Photonics, Graefling, Germany) equipped with a motorized sample stage, a polychrome V (Till Photonics), a 40x objective (alpha Plan Fluar 40x, Zeiss, Göttingen, Germany) and a charge-coupled device camera (AVT Stingray F145B, Allied Vision Technologies, Stadtroda, Germany) was used. The FRET-based mitochondrial Ca^{2+} sensor 4mtD3cpV was excited at 430 nm and emission was collected using the dichrotome dual emission filter set (dichroic 535dcxr, CFP emitter 482/18 nm and YFP emitter 535/3 nm). TMRM was visualized at an excitation of 550 nm and emission of 575 nm. For monitoring $NO^{\bullet}$ dynamics G-geNOp expressing cells were exposed to 480 nm and emitted at 515 nm. For simultaneous measurements of cytosolic $Ca^{2+}$and $NO^{\bullet}$, fura-2/am loaded and G-geNOp expressing cells were alternately excited at 340, 380 and 480 nm, respectively and emission was recorded at 515 nm (515dcxr). Data acquisition and control was carried out by the Live Acquisition 2.0.0.12 software (Till Photonics). Confocal imaging of adenoviral infected G-geNOp expressing EA.hy926 or transient transfected eNOS-RFP expressing HEK293 cells was performed as described previously by using a 40× objective (Plan-Neofluar 40×/1.3 oil, Zeiss) or a 100× objective (Plan-Fluar 100×/1.45 oil, Zeiss), respectively [17].

2.5 Immunoblotting

Transfected EA.hy926 cells (siControl, siMCU/EMRE or siMICU1) were incubated with vehicle (water) or 100 μM ATP at 37 °C for 3 or 5 min. Cells were then harvested and homogenized by sonication (3×5 s) in ice-cold RIPA lysis buffer (Sigma, Vienna, Austria) containing 2 mM EDTA, protease and phosphatase inhibitors (CompleteTM, PhosSTOPTM, Roche, Vienna, Austria). Protein concentration was determined with the PierceTM BCA Protein Assay Kit using bovine serum albumin as standard (Fisher Scientific Austria GmbH, Vienna, Austria). Denatured samples (30 μg) were separated by SDS-PAGE on 10% gels and transferred electrophoretically to nitrocellulose membranes. After blocking with 5% non- fat dry milk in Tris-buffered saline containing 0.1% (v/v) TWEEN-20 for 1 h, membranes were incubated overnight at 4 °C with a primary antibody against eNOS (1:2000; BD Transduction Laboratories), Ser^{1177} phospho-eNOS (1:1000; BD Transduction Laboratories) or β-actin (1:200,000; Sigma). Thereafter, membranes were washed 3 times and incubated for 1 h with a horseradish peroxidase-conjugated anti-mouse IgG secondary antibody (1:5000). Immunoreactive bands were visualized by chemiluminescence using ECL

detection reagent (Biozym, Germany) and quantified densitometrically using the Fusion SL system (Peqlab, Erlangen, Germany).

2.6 Statistical analyses

The acquired data were analyzed by the GraphPad Prism software version 5.04 (GraphPad Software, San Diego, CA, USA). Data are presented as mean ± standard error of mean (SEM) of independent experiments (N) throughout the whole manuscript. For comparisons between two groups, two-tailed Student *t*-test was used for evaluation of statistical significance and a p value between 0.01 and 0.05 (pStudent´s *t*-test) was considered significant and indicated with "*", p between 0.001 and 0.01 as very significant with "**" and $p < 0.001$ as highly significant with "***". For comparisons across multiple groups, one-way ANOVA with Barlett's test for equal variances and Tukey's Multiple Comparision test were used for evaluating statistical significance expressed as described above. Data shown are either average or representative curves of at least three independent experiments, including analyses from imaging and western blot experiments.

3 Results

3.1 Real-time monitoring of $NO^{\bullet}$ production in single endothelial cells

To monitor single cell $NO^{\bullet}$ dynamics in EA.hy926 cells we used the novel geNOp technology [15]. The geNOps are protein-based fluorescent $NO^{\bullet}$ reporters that immediately and specifically respond to physiological cellular $NO^{\bullet}$ elevations by fluorescence quenching in a reversible manner (Fig. 1A). Adenoviral transduction resulted in very high numbers of geNOp-positive EA.hy926 cells (Fig. 1B). To elucidate $NO^{\bullet}$ production in response to Ca^{2+} release from the endoplasmic reticulum (ER), endothelial cells expressing G-geNOp (green-geNOp) were first stimulated with the inositol 1,4,5-trisphosphate (IP_3)-generating agonist ATP in the absence of extracellular Ca^{2+}. Under these conditions ATP evoked a transient $NO^{\bullet}$ signal in endothelial cells (Fig. 1C-D). Cytosolic $NO^{\bullet}$ levels recovered rapidly upon the subsequent addition of Ca^{2+} to ATP stimulated cells and remained elevated in the presence of the IP_3-generating agonist (Fig. 1C-D). These findings demonstrate the importance of Ca^{2+} entry for sustained eNOS activation in EA.hy926 cells. However, within a few minutes elevated $NO^{\bullet}$ signals gradually decreased back to basal levels upon the washout of ATP (Fig. 1C-D).

The geNOp signals were abolished in the presence of L-N^{G}-nitro arginine, a potent eNOS inhibitor [18], which did not affect respective cytosolic Ca^{2+} elevations (Supplementary data – Fig. 1). To further confirm the specificity of the G-geNOp signals, endothelial cells expressing the $NO^{\bullet}$ insensitive mutated version of G-geNOp, referred to as G-geNOp^{mut}, were investigated. Cell treatment with the IP_3-generating agonist ATP did not evoke significant fluorescence signals in cells expressing G-geNOp^{mut} (Supplementary data – Fig. 2), demonstrating that geNOps do not report intracellular pH changes under these experimental conditions [15]. As the $NO^{\bullet}$ probe did not respond to $NO^{\bullet}$ related species such as nitrite, nitrate [14], H_2S (Supplementary data – Fig. 3) and other $NO^{\bullet}$ related compounds [15], these experiments confirm that geNOp-expressing EA.hy926 cells represent a suitable model to specifically study Ca^{2+}-triggered eNOS-dependent generation of $NO^{\bullet}$ on the level

of individual cells. The simultaneous measurement of $NO^{\bullet}$ and Ca^{2+} in the same single cell unveiled that cellular $NO^{\bullet}$ dynamics strictly follow respective Ca^{2+} signals (Fig. 1D), indicating that $NO^{\bullet}$ production in EA.hy926 cells is primarily controlled by the free cytosolic Ca^{2+} concentration ($[Ca^{2+}]_{cyto}$).

3.2 Genetic ablation of mitochondrial Ca^{2+} uptake reduces eNOS-mediated $NO^{\bullet}$ formation

Next we set out to investigate how mitochondrial Ca^{2+} uptake affects $NO^{\bullet}$ production in endothelial cells. For this purpose EA.hy926 cells were treated with siRNA against both MCU and EMRE, two recently identified key components of the mitochondrial Ca^{2+} uniporter pore [9,19]. In line with other reports [13,20–22], the siRNA-mediated knock-down of these proteins substantially reduced mitochondrial Ca^{2+} signals in response to ER Ca^{2+} release and Ca^{2+} entry, while the basal mitochondrial Ca^{2+} levels were only slightly reduced (Fig. 2A). Under the same experimental conditions global cytosolic Ca^{2+} signals were only diminished at the plateau phase upon Ca^{2+} addition (Fig. 2B), confirming that mitochondrial Ca^{2+} uptake facilitates store operated Ca^{2+} entry (SOCE) in endothelial cells [20,23,24]. However, cells ablated from MCU and EMRE showed considerably reduced $NO^{\bullet}$ production upon Ca^{2+} mobilization in the absence and presence of Ca^{2+} entry (Fig. 2C). As expected both control cells and cells treated with siRNA against MCU and EMRE did not show significant changes of the fluorescence signal of the $NO^{\bullet}$-insensitive G-geNOp^{mut} in response to ATP (Fig. 2C, right panel). Compared to respective control cells, the Ca^{2+}-triggered $NO^{\bullet}$ signals were significantly reduced in MCU- and EMRE silenced EA.hy926 cells that were stimulated with either 1 μM, 5 μM or 100 μM ATP (Fig. 2D), indicating that mitochondrial Ca^{2+} uptake is relevant for eNOS activation over a broad range of physiological and supra-physiological levels of Ca^{2+} mobilization.

In order to investigate if silencing of MCU and EMRE also impacts on Ca^{2+}-triggered $NO^{\bullet}$ production in non-immortalized endothelial cells, primary human umbilical vein endothelial cells (HUVEC) were tested. HUVECs pooled from different donors showed more transient cytosolic Ca^{2+} signals in response to ATP compared to EA.hy926 cells, while the basal cytosolic Ca^{2+} levels were identical in both cell types (Fig. 3A). Respective mitochondrial Ca^{2+} elevations tended to be stronger in the primary endothelial cells (Fig. 3B). In average the ATP-evoked $NO^{\bullet}$ signals in HUVECs expressing G-geNOp (Fig. 3C) were less pronounced and occurred with rather slow kinetics compared to the faster and stronger $NO^{\bullet}$ elevations in EA.hy926 cells (Fig. 3C). Nevertheless, the knock down of MCU and EMRE, which reduced mitochondrial Ca^{2+} signals in HUVECs (Fig. 3D), also resulted in diminished ATP-evoked $NO^{\bullet}$ formation in the primary endothelial cells (Fig. 3E). The siRNA-mediated knock-down of MCU and EMRE significantly reduced both the amplitude and slope of ATP-triggered $NO^{\bullet}$ signals in HUVECs (Fig. 3E).

3.3 Mitochondrial depolarization reduces Ca^{2+}-triggered $NO^{\bullet}$ formation in EA.hy926 cells

The impact of impaired mitochondrial Ca^{2+} uptake was studied by depolarization of the mitochondrial membrane potential with a combination of oligomycin and antimycin (Fig. 4A and B). In the presence of these compounds the Ca^{2+}-triggered $NO^{\bullet}$ signal was significantly reduced in response to Ca^{2+} release and entry (Fig. 4C). The fluorescence signal of the $NO^{\bullet}$-insensitive G-geNOp^{mut} remained unaffected by oligomycin and

antimycin independently of the presence of Ca^{2+}(Fig. 4C, **right panel**). Under the same experimental conditions cytosolic Ca^{2+} signals were, however, only partially reduced during Ca^{2+} addition (Fig. 4D). These findings again indicate that mitochondrial Ca^{2+} signals positively regulate eNOS activity.

3.4 Genetic augmentation of mitochondrial Ca^{2+} uptake increases eNOS-mediated $NO^{\bullet}$ formation

We next investigated whether Ca^{2+}-evoked $NO^{\bullet}$ production is gradable by increasing mitochondrial Ca^{2+} uptake. For this purpose the expression level of MICU1, a negative regulator of mitochondrial Ca^{2+} uptake [10], was silenced by siRNA in EA.hy926 cells. As expected, cells treated with siRNA against MICU1 showed increased basal mitochondrial Ca^{2+} levels and ATP-evoked Ca^{2+} uptake in the absence and presence of extracellular Ca^{2+}(Fig. 5A). Respective global cytosolic Ca^{2+} elevations remained almost unaffected by the knock-down of MICU1 (Fig. 5B). However, the Ca^{2+}-triggered $NO^{\bullet}$ production was significantly higher in the MICU1-depleted EA.hy926 cells upon both Ca^{2+} release and entry (Fig. 5C), emphasizing that increasing mitochondrial Ca^{2+} uptake augments $NO^{\bullet}$ production. The fluorescence signal of the $NO^{\bullet}$-insensitive G-geNOp^{mut} remained unaffected by cell treatment with the IP_3-generating agonist independently of MICU1 expression (Fig. 5C, **right panel**). In primary HUVECs siRNA-mediated silencing of MICU1 also increased mitochondrial Ca^{2+} signals in response to ATP (Fig. 5D). However, the ATP-induced $NO^{\bullet}$ formation (Fig. 5D) was only slightly increased in HUVECs that had been treated with siRNA against MICU1 compared to respective control cells (Fig. 5E).

3.5 The eNOS expression levels as well as basal and ATP-stimulated eNOS phosphorylation remain unaffected by silencing MCU, EMRE or MICU1

Phosphorylation of several sites within the eNOS protein significantly modulates its activity [25]. Particularly, eNOS phosphorylation at serine^{1177} is known to enhance its activity [25,26]. Accordingly, we performed western blot analysis using EA.hy926 cells to investigate whether or not the knock-down of MCU/EMRE and MICU1 affects eNOS phosphorylation at serine^{1177}. As shown in Fig. 6 the knock-down of neither MCU/EMRE nor MICU1 affected eNOS phosphorylation under basal (unstimulated) conditions. Cell treatment with ATP raised eNOS phosphorylation levels within 3 and 5 min (Fig. 6), while the ATP-induced increase of phosphorylated eNOS (peNOS) was not altered by MCU/EMRE and MICU1 silencing (Fig. 6). In line with these findings the expression of eNOS in EA.hy926 cells was not affected by knock-down of MCU/EMRE or MICU1 (total eNOS, Fig. 6A). These findings again confirm that mitochondrial Ca^{2+} uptake supports $NO^{\bullet}$ production in endothelial cells without affecting the global cytosolic Ca^{2+} concentration, eNOS-expression levels and phosphorylation at serine^{1177}.

3.6 Mitochondrial Ca^{2+} uptake significantly contributes to Ca^{2+}-triggered $NO^{\bullet}$ formation in HEK293 cells transiently expressing eNOS-RFP

There is general agreement that eNOS is mainly localized at the plasma membrane [27]. However, in a previous study it has been suggested that mitochondrial Ca^{2+} uptake stimulates $NO^{\bullet}$ formation by a mitochondrial NOS isoform in bovine endothelial cells [5].

Therefore, we transiently expressed wild-type eNOS-RFP in HEK293 cells, which do not express any NOS isoforms. Confocal microscopy of eNOS-RFP expressing HEK293 cells confirmed that the NO•-generating enzyme is located predominately at the plasma membrane and intracellular vesicular structures but not within mitochondria of cells (Fig. 7A). HEK293 cells expressing eNOS-RFP showed a considerable increase of cellular NO• levels in response to the IP_3-generating agonist ATP (Fig. 7B). Control cells which were not transfected with eNOS-RFP were unable to produce NO• upon the addition of the agonist (Fig. 7B). However, the response of the NO• probe to the NO•-donor sodium nitroprusside (SNP) was the same in both control (HEK) and eNOS-RFP expressing HEK293 cells (HEK + eNOS-RFP) (Fig. 7B). Knock-down of MCU/EMRE in HEK293 cells significantly reduced mitochondrial Ca^{2+} signals in response to ATP (Fig. 7C), while the respective cytosolic Ca^{2+} elevation remained unaffected by silencing these MCU components (Fig. 7D). As expected, knock-down of MICU1 resulted in increased mitochondrial Ca^{2+}- levels and uptake without affecting respective cytosolic Ca^{2+} signals (Fig. 7C and D). In line with our results using primary endothelial cells ATP-evoked NO•-signals were significantly reduced in cells silenced of MCU and EMRE (Fig. 7E), while MICU1 silencing only marginally increased respective NO• signals in HEK293 cells expressing eNOS-RFP.

4 Discussion

Taking advantage of the novel genetically encoded fluorescent NO• probes [15] and the knowledge of recently identified key components of mitochondrial Ca^{2+} channels, we could specifically investigate the impact of mitochondrial Ca^{2+} uptake on eNOS-mediated NO• formation on the level of individual cells. Our data show a positive association of mitochondrial Ca^{2+} signals and NO• production upon cell treatment with a physiological Ca^{2+}-mobilizing agonist and, hence, emphasize that mitochondrial Ca^{2+} uptake promotes the Ca^{2+}-triggered biosynthesis of this vasoactive molecule by eNOS.

Our simultaneous recordings of Ca^{2+} and NO• signals confirm that the Ca^{2+}/calmodulin-dependent activation mechanism of the eNOS [7] is under the control of the global cytosolic Ca^{2+} concentration [28,29]. However, genetic manipulations of the mitochondrial Ca^{2+} uptake capacity markedly attenuated the ATP-evoked NO• formation without affecting global cytosolic Ca^{2+} signals. These observations strongly indicate that mitochondrial Ca^{2+} uptake contributes to the regulation of eNOS activity. Several data point to a localization of eNOS or other NOS isoforms within mitochondria or at their surface [5,30–33]. It has been suggested that mitochondrial Ca^{2+} uptake stimulates NO• formation within mitochondria of calf pulmonary artery endothelial cells by a mitochondria-specific NOS isoform [5]. The positive association between mitochondrial Ca^{2+} uptake and NO• generation, found in the present study, is in line with the concept of Ca^{2+}-dependent mitochondria targeted NOS isoforms [5,34,35]. However, because of the lack of a clear proof, the existence of mitochondria-specific NOS isoforms in endothelial cells remains an issue of debate [36]. While we did not investigate whether or not a mitochondria located NOS is present in EA.hy926 cells and HUVECs, our data with HEK293 cells expressing eNOS-RFP indicate that mitochondrial Ca^{2+} uptake contributes to eNOS activity even if the enzyme is outside the organelle. It is, hence, feasible, that mitochondria in the vicinity of extra-mitochondrial NOS might positively control the cellular NO• production by shaping the patterns of local

Ca^{2+} signals [24] and/or contributing to the availability of essential NOS cofactors [37]. Further experiments are necessary to clarify by which molecular mechanisms mitochondrial Ca^{2+} uptake supports $NO^{\bullet}$ production by eNOS. In this study we could, however, exclude that eNOS phosphorylation at $serine^{1177}$, which is known to enhance eNOS activity [25,26], is under the control of mitochondrial Ca^{2+} uptake. Cell treatment with ATP significantly increased eNOS phosphorylation at $serine^{1177}$. This finding is in line with other reports that demonstrated interrelations between the Ca^{2+}/calmodulin- and phosphorylation-dependent activation of eNOS [25,26]. Different cellular kinases such as the AMPK [38], PKC delta [39] or the PI3K/Akt pathway [40,41] might be responsible for the ATP-dependent phosphorylation of eNOS at $serine^{1177}$ in EA.hy926 cells.

Our results strongly suggest that targeting the mitochondrial Ca^{2+} homeostasis represents a promising approach to therapeutically intervene in endothelium-governed $NO^{\bullet}$-dependent vasoreactivity. However, the availability of pharmacological tools that specifically target the MCU machinery is very limited. We used a combination of oligomycin, an inhibitor of the ATP synthase, and antimycin, an inhibitor of complex III, in order to abolish mitochondrial Ca^{2+} uptake indirectly. This kind of cell treatment strongly affects the metabolic activity of the organelle and can lead to a severe cellular ATP depletion [42], which in turn affects the local and global cellular Ca^{2+} homeostasis [24]. While our data show that cell treatment with the mitochondria depolarizing compounds reduces eNOS-mediated $NO^{\bullet}$ production in response to the IP_3-generating agonist in EA.hy926 cells, the molecular mechanisms responsible for this effect on eNOS activity might be different from those in cells with reduced levels of MCU components. Due to the lack of suitable agents that specifically target the mitochondrial Ca^{2+} homeostasis, the impact of an acute alteration of mitochondrial Ca^{2+} fluxes on eNOS activity is difficult to investigate. It is possible that the siRNA-mediated knock-down of components of the MCU machinery introduces secondary effects on the cellular bioenergetics that may interfere with eNOS function. Such effects cannot be ruled out, although other studies have demonstrated that silencing or even the knock-out of MCU components have surprisingly little impact on the cellular metabolic homeostasis *in situ* [12] and *in vivo* [43,44]. Eventually, our data suggest that manipulating mitochondrial Ca^{2+} uptake may represent an attractive strategy for controlling the eNOS/$NO^{\bullet}$-dependent vascular reactivity. Nevertheless, the molecular mechanism linking mitochondrial Ca^{2+} uptake to eNOS function and/or $NO^{\bullet}$ bioavailability remains to be clarified in more detail.

Supplementary Material

Refer to Web version on PubMed Central for supplementary material.

Acknowledgements

We thank Margarete Lechleitner, Anna Schreilechner and Dr. Rene Rost for their excellent technical assistance and Dr. C.J.S. Edgell (University of North Carolina, Chapel Hill, NC, USA) for providing the EA.hy926 cells. Moreover we thank Professor Roger Tsien (University of California San Diego, CA, USA) for providing 4mtD3cpv. Special thanks to the team of NGFI (Next Generation Fluorescence Imaging GmbH, Graz, Austria, http://www.ngfi.eu/) for optimizing the infection protocol with the G-geNOp adenovirus.

Sources of funding

E.E. is supported by Nikon Austria within the Nikon-Center of Excellence Graz. E.E. and M.R.D. are fellows of the PhD program Molecular Medicine (MOLMED) at the Medical University of Graz. This work was also funded by the FWF project P 28529B27 at the Medical University of Graz. C.T.M.-S. is funded by the FWF within the PhD Program Metabolic and Cardiovascular Disease (DK-W1226). S.C. holds an academic development scholarship from the University of Phayao (Phayao, Thailand) and is a student of the doctoral school Molecular Medicine and Inflammation of the Medical University of Graz. Microscopic equipment is part of the Nikon-Center of Excellence Graz that is supported by the Austrian infrastructure program 2013/2014, Nikon Austria Inc., and BioTechMed-Graz.

Nonstandard Abbreviations and Acronyms

Ψ_{mito}	mitochondrial membrane potential
EMRE	essential mitochondrial calcium uniporter regulator
eNOS	endothelial nitric oxide synthase
geNOps	genetically encoded fluorescent nitric oxide probes
EGFP	enhanced green fluorescent protein
ER	endoplasmic reticulum
IP_3	inositol 1,4,5-trisphosphate
MCU	mitochondrial calcium uniporter
MICU1	mitochondrial calcium uptake 1
$NO^{\bullet}$	nitric oxide
P-eNOS	phosphorylated endothelial nitric oxide synthase
RFP	red fluorescent protein
SOCE	store operated Ca^{2+} entry
TMRM	tetramethylrhodamine methyl ester perchlorate

References

[1]. Denton RM. Regulation of mitochondrial dehydrogenases by calcium ions. Biochim Biophys Acta. 1787; 2009:1309–1316.

[2]. Bhosale G, Sharpe JA, Sundier SY, Duchen MR. Calcium signaling as a mediator of cell energy demand and a trigger to cell death. Ann N Y Acad Sci. 2015; 1350:107–116. [PubMed: 26375864]

[3]. Rimessi A, Giorgi C, Pinton P, Rizzuto R. The versatility of mitochondrial calcium signals: from stimulation of cell metabolism to induction of cell death. Biochim Biophys Acta. 1777; 2008:808–816.

[4]. Graier WF, Frieden M, Malli R. Mitochondria and Ca^{2+} signaling: old guests, new functions. Pflug Arch. 2007; 455:375–396.

[5]. Dedkova EN, Ji X, Lipsius SL, Blatter LA. Mitochondrial calcium uptake stimulates nitric oxide production in mitochondria of bovine vascular endothelial cells. Am J Physiol Cell Physiol. 2004; 286:406–415.

[6]. Dromparis P, Michelakis ED. Mitochondria in vascular health and disease. Annu Rev Physiol. 2013; 75:95–126. [PubMed: 23157555]

Europe PMC Funders Author Manuscripts

[7]. Fleming I. Molecular mechanisms underlying the activation of eNOS. Pflug Arch. 2010; 459:793–806.

[8]. Ghafourifar P, Parihar MS, Nazarewicz R, Zenebe WJ, Parihar A. Detection assays for determination of mitochondrial nitric oxide synthase activity; advantages and limitations. Meth Enzym. 2008; 440:317–334. [PubMed: 18423228]

[9]. Baughman JM, Perocchi F, Girgis HS, Plovanich M, Belcher-Timme CA, Sancak Y, Bao XR, Strittmatter L, Goldberger O, Bogorad RL, Koteliansky V, et al. Integrative genomics identifies MCU as an essential component of the mitochondrial calcium uniporter. Nature. 2011; 476:341–345. [PubMed: 21685886]

[10]. Mallilankaraman K, Doonan P, Cardenas C, Chandramoorthy HC, Muller M, Miller R, Hoffman NE, Gandhirajan RK, Molgo J, Birnbaum MJ, Rothberg BS, et al. MICU1 is an essential gatekeeper for MCU-mediated mitochondrial Ca^{2+} uptake that regulates cell survival. Cell. 2012; 151:630–644. [PubMed: 23101630]

[11]. Csordas G, Golenar T, Seifert EL, Kamer KJ, Sancak Y, Perocchi F, Moffat C, Weaver D, de la Fuente Perez S, Bogorad R, Koteliansky V, et al. MICU1 controls both the threshold and cooperative activation of the mitochondrial Ca^{2+} uniporter. Cell Metab. 2013; 17:976–987. [PubMed: 23747253]

[12]. Madreiter-Sokolowski CT, Klec C, Parichatikanond W, Stryeck S, Gottschalk B, Pulido S, Rost R, Eroglu E, Hofmann NA, Bondarenko AI, Madl T, et al. PRMT1-mediated methylation of MICU1 determines the UCP2/3 dependency of mitochondrial Ca^{2+} uptake in immortalized cells. Nat Commun. 2016; 7:e12897.

[13]. Waldeck-Weiermair M, Malli R, Parichatikanond W, Gottschalk B, Madreiter-Sokolowski CT, Klec C, Rost R, Graier WF. Rearrangement of MICU1 multimers for activation of MCU is solely controlled by cytosolic Ca^{2+} Sci Rep. 2015; 5:e15602.

[14]. Opelt M, Eroglu E, Waldeck-Weiermair M, Russwurm M, Koesling D, Malli R, Graier WF, Fassett JT, Schrammel A, Mayer B. Formation of nitric oxide by aldehyde dehydrogenase-2 is necessary and sufficient for vascular bioactivation of nitroglycerin. J Biol Chem. 2016 (Epub ahead of print).

[15]. Eroglu E, Gottschalk B, Charoensin S, Blass S, Bischof H, Rost R, Madreiter-Sokolowski CT, Pelzmann B, Bernhart E, Sattler W, Hallstrom S, et al. Development of novel FP-based probes for live-cell imaging of nitric oxide dynamics. Nat Commun. 2016; 7:e10623.

[16]. Edgell CJ, McDonald CC, Graham JB. Permanent cell line expressing human factor VIII-related antigen established by hybridization. Proc Natl Acad Sci USA. 1983; 80:3734–3737. [PubMed: 6407019]

[17]. Waldeck-Weiermair M, Bischof H, Blass S, Deak AT, Klec C, Graier T, Roller C, Rost R, Eroglu E, Gottschalk B, Hofmann NA, et al. Generation of red-shifted cameleons for imaging Ca^{2+} dynamics of the endoplasmic reticulum. Sensors. 2015; 15:13052–13068. [PubMed: 26053751]

[18]. Griffith OW, Kilbourn RG. Nitric oxide synthase inhibitors: amino acids. Meth Enzym. 1996; 268:375–392. [PubMed: 8782604]

[19]. Sancak Y, Markhard AL, Kitami T, Kovacs-Bogdan E, Kamer KJ, Udeshi ND, Carr SA, Chaudhuri D, Clapham DE, Li AA, Calvo SE, et al. EMRE is an essential component of the mitochondrial calcium uniporter complex. Science. 2013; 342:1379–1382. [PubMed: 24231807]

[20]. Deak AT, Blass S, Khan MJ, Groschner LN, Waldeck-Weiermair M, Hallstrom S, Graier WF, Malli R. IP_3-mediated STIM1 oligomerization requires intact mitochondrial Ca^{2+} uptake. J Cell Sci. 2014; 127:2944–2955. [PubMed: 24806964]

[21]. Bondarenko AI, Jean-Quartier C, Parichatikanond W, Alam MR, Waldeck-Weiermair M, Malli R, Graier WF. Mitochondrial, Ca^{2+} uniporter (MCU)-dependent and MCU-independent Ca^{2+} channels coexist in the inner mitochondrial membrane. Pflug Arch. 2014; 466:1411–1420.

[22]. Bondarenko AI, Parichatikanond W, Madreiter CT, Rost R, Waldeck-Weiermair M, Malli R, Graier WF. UCP2 modulates single-channel properties of a MCU-dependent Ca^{2+} inward current in mitochondria. Pflug Arch. 2015; 467:2509–2518.

[23]. Naghdi S, Waldeck-Weiermair M, Fertschai I, Poteser M, Graier WF, Malli R. Mitochondrial Ca^{2+} uptake and not mitochondrial motility is required for STIM1-Orai1-dependent store-operated Ca^{2+} entry. J Cell Sci. 2010; 123:2553–2564. [PubMed: 20587595]

[24]. Malli R, Frieden M, Osibow K, Zoratti C, Mayer M, Demaurex N, Graier WF. Sustained Ca^{2+} transfer across mitochondria is Essential for mitochondrial Ca^{2+} buffering, store-operated Ca^{2+} entry, and Ca2+ store refilling. J Biol Chem. 2003; 278:44769–44779. [PubMed: 12941956]

[25]. Fulton D, Gratton JP, Sessa WC. Post-translational control of endothelial nitric oxide synthase: why isn't calcium/calmodulin enough? J Pharmacol Exp Ther. 2001; 299:818–824. [PubMed: 11714864]

[26]. Dimmeler S, Fleming I, Fisslthaler B, Hermann C, Busse R, Zeiher AM. Activation of nitric oxide synthase in endothelial cells by Akt-dependent phosphorylation. Nature. 1999; 399:601–605. [PubMed: 10376603]

[27]. Villanueva C, Giulivi C. Subcellular and cellular locations of nitric oxide synthase isoforms as determinants of health and disease. Free Radic Biol Med. 2010; 49:307–316. [PubMed: 20388537]

[28]. Luckhoff A, Pohl U, Mulsch A, Busse R. Differential role of extra- and intracellular calcium in the release of EDRF and prostacyclin from cultured endothelial cells. Br J Pharm. 1988; 95:189–196.

[29]. Graier WF, Schmidt K, Kukovetz WR. Effect of sodium fluoride on cytosolic free Ca^{2+}-concentrations and cGMP-levels in endothelial cells. Cell Signal. 1990; 2:369–375. [PubMed: 2174691]

[30]. Zaobornyj T, Ghafourifar P. Strategic localization of heart mitochondrial NOS: a review of the evidence. Am J Physiol Heart Circ Physiol. 2012; 303:1283–1293.

[31]. Nazarewicz RR, Zenebe WJ, Parihar A, Parihar MS, Vaccaro M, Rink C, Sen CK, Ghafourifar P. 12(S)-hydroperoxyeicosatetraenoic acid (12-HETE) increases mitochondrial nitric oxide by increasing intramitochondrial calcium. Arch Biochem Biophys. 2007; 468:114–120. [PubMed: 17963719]

[32]. Valdez LB, Boveris A. Mitochondrial nitric oxide synthase, a voltage-dependent enzyme, is responsible for nitric oxide diffusion to cytosol. Front Biosci. 2007; 12:1210–1219. [PubMed: 17127374]

[33]. Parihar MS, Parihar A, Villamena FA, Vaccaro PS, Ghafourifar P. Inactivation of mitochondrial respiratory chain complex I leads mitochondrial nitric oxide synthase to become pro-oxidative. Biochem Biophys Res Commun. 2008; 367:761–767. [PubMed: 18191636]

[34]. Traaseth N, Elfering S, Solien J, Haynes V, Giulivi C. Role of calcium signaling in the activation of mitochondrial nitric oxide synthase and citric acid cycle. Biochim Biophys Acta. 1658; 2004:64–71.

[35]. Valdez LB, Zaobornyj T, Boveris A. Mitochondrial metabolic states and membrane potential modulate mtNOS activity. Biochim Biophys Acta. 1757; 2006:166–172.

[36]. Lacza Z, Pankotai E, Busija DW. Mitochondrial nitric oxide synthase: current concepts and controversies. Front Biosci. 2009; 14:4436–4443.

[37]. Shaul PW. Regulation of endothelial nitric oxide synthase: location, location, location. Annu Rev Physiol. 2002; 64:749–774. [PubMed: 11826287]

[38]. Chen ZP, Mitchelhill KI, Michell BJ, Stapleton D, Rodriguez-Crespo I, Witters LA, Power DA, Ortiz de Montellano PR, Kemp BE. AMP-activated protein kinase phosphorylation of endothelial NO synthase. FEBS Lett. 1999; 443:285–289. [PubMed: 10025949]

[39]. da Silva CG, Specht A, Wegiel B, Ferran C, Kaczmarek E. Mechanism of purinergic activation of endothelial nitric oxide synthase in endothelial cells. Circulation. 2009; 119:871–879. [PubMed: 19188511]

[40]. Bauer PM, Fulton D, Boo YC, Sorescu GP, Kemp BE, Jo H, Sessa WC. Compensatory phosphorylation and protein-protein interactions revealed by loss of function and gain of function mutants of multiple serine phosphorylation sites in endothelial nitric-oxide synthase. J Biol Chem. 2003; 278:14841–14849. [PubMed: 12591925]

[41]. Harris MB, Ju H, Venema VJ, Liang H, Zou R, Michell BJ, Chen ZP, Kemp BE, Venema RC. Reciprocal phosphorylation and regulation of endothelial nitric-oxide synthase in response to bradykinin stimulation. J Biol Chem. 2001; 276:16587–16591. [PubMed: 11340086]

[42]. Vishnu N, Jadoon Khan M, Karsten F, Groschner LN, Waldeck-Weiermair M, Rost R, Hallstrom S, Imamura H, Graier WF, Malli R. ATP increases within the lumen of the endoplasmic reticulum upon intracellular Ca^{2+} release. Mol Biol Cell. 2014; 25:368–379. [PubMed: 24307679]

[43]. Pendin D, Greotti E, Pozzan T. The elusive importance of being a mitochondrial Ca^{2+} uniporter. Cell Calcium. 2014; 55:139–145. [PubMed: 24631327]

[44]. Pan X, Liu J, Nguyen T, Liu C, Sun J, Teng Y, Fergusson MM, Rovira II, Allen M, Springer DA, Aponte AM, et al. The physiological role of mitochondrial calcium revealed by mice lacking the mitochondrial calcium uniporter. Nat Cell Biol. 2013; 15:1464–1472. [PubMed: 24212091]

Europe PMC Funders Author Manuscripts

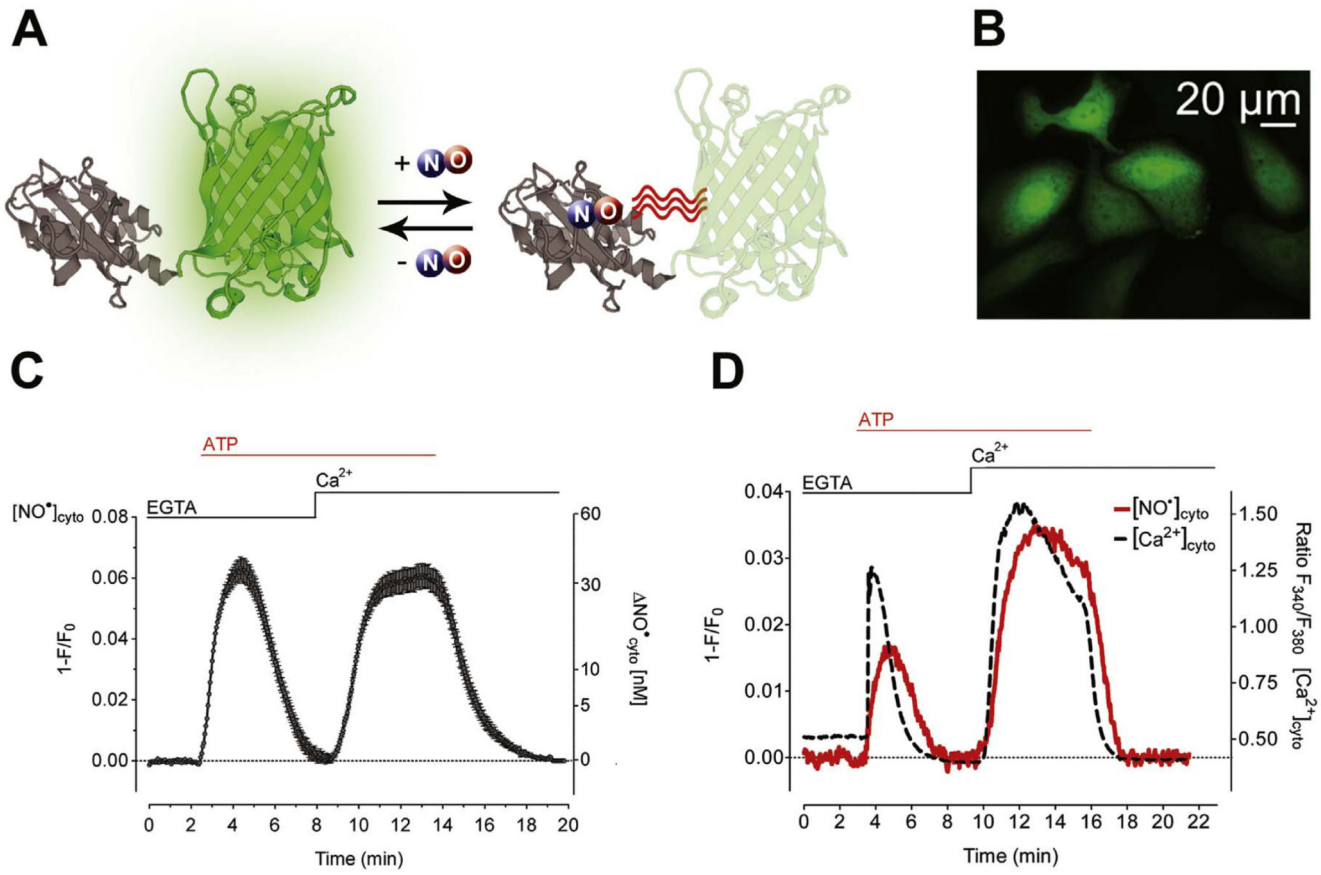

Fig. 1. Live-cell imaging of Ca^{2+}-triggered $NO^{\bullet}$ formation in endothelial cells expressing G-geNOp.

(A) Schematic illustration of G-geNOp consisting of the enhanced green fluorescent protein (EGFP) fused to the bacteria-derived $NO^{\bullet}$ binding domain GAF (grey). Binding of $NO^{\bullet}$ in the vicinity of EGFP in G-geNOp induces fluorescence quenching. (B) Representative image showing EA.hy926 cells expressing G-geNOp. Notably, the $NO^{\bullet}$ probe localizes to the nucleus and cytosol. (C) Average curve (± SEM) showing $NO^{\bullet}$ signal over time obtained from single EA.hy926 cells obtained from independent experiments (N =40) upon treatment with 100 µM ATP in the absence of Ca^{2+}(1 mM EGTA) and upon Ca^{2+}(2 mM) addition. (D) Representative simultaneous recordings of $NO^{\bullet}$ (solid grey line) and Ca^{2+}(dashed black line) signals over time in a single fura-2/am loaded EA.hy926 cell expressing G-geNOp. As indicated the cell was treated with 100 µM ATP in the absence of Ca^{2+}(1 mM EGTA) and upon Ca^{2+} addition (2 mM) for 14 min.

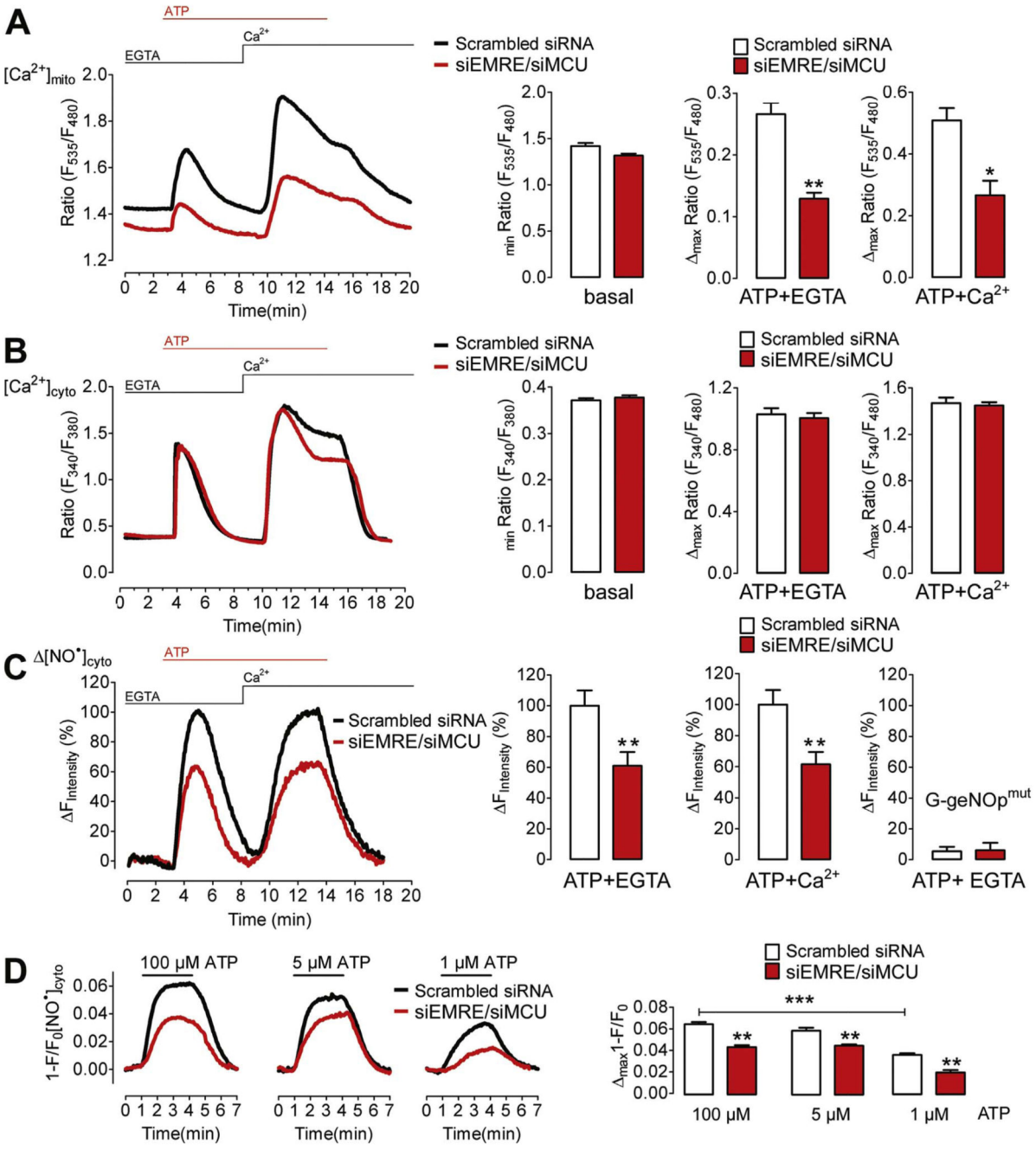

Fig. 2. Knock-down of EMRE and MCU reduces Ca^{2+}-triggered $NO^{\bullet}$ production in EA.hy926 cells.

(A) Average curves of $[Ca^{2+}]_{mito}$ (left panel) in EA.hy926 cells treated with either scrambled siRNA (black curve and white bars, N=3) or siRNAs against EMRE and MCU (siEMRE/siMCU, red curve and red bars, N=3) upon stimulation with 100 μM ATP in the absence of extracellular Ca^{2+}(1 mM EGTA) followed by addition of Ca^{2+}(2 mM). Bar graphs showing average basal Ca^{2+} level (basal, p=0.0581) and Ca^{2+} transients in response to 100 μM ATP-stimulated ER Ca^{2+} release (ATP + EGTA, **p=0.0029) and store-operated Ca^{2+} entry (ATP + Ca^{2+}, *p=0.0169). (B) Curves representing average of $[Ca^{2+}]_{cyto}$ in control (Scrambled

Europe PMC Funders Author Manuscripts

siRNA, black curve, N=6) versus EMRE/MCU ablated (siEMRE/siMCU, red curve, N=7) EA.hy926 cells (left panel) stimulated with 100 μM ATP in the absence (1 mM EGTA) and addition of Ca^{2+}(2 mM) as indicated. Respective statistical analyses of basal levels (basal, p=0.397), maximum cytosolic Ca^{2+} release (ATP + EGTA, p=0.6373) and maximum cytosolic Ca^{2+} entry (ATP + Ca^{2+}, p=0.6988). (C) Representative curve of $[NO^{\bullet}]_{cyto}$ in response to ATP stimulation. Statistical analyses of average $[NO^{\bullet}]_{cyto}$ are shown in bar graphs (right panels). Maximal signals (amplitude) of scrambled siRNA- or siMCU/siEMRE-treated cells are defined as 100%. Cells were first stimulated with 100 μM ATP in the absence of extracellular Ca^{2+} in control cells (Scrambled siRNA, white column, ATP + EGTA, N =17) and cells reduced of EMRE and MCU (siEMRE/siMCU, red column, ATP + EGTA, N =17) and upon Ca^{2+}(2 mM) addition (right middle column pair). **p=0.0068 (ATP+EGTA) and **p=0.0042 (ATP+Ca^{2+}) vs Scrambled siRNA. Right columns represent maximal fluorescence changes of G-geNOp^{mut} in response to 100 μM ATP in EGTA (1 mM) in control cells (white column, N =11) and cells treated with siRNA against EMRE and MCU (red column, N =10). (D) Average curves of Ca^{2+}-dependent NO formation upon stimulation with 1 μM (upper left panel) 5 μM (upper middle panel) or 100 μM ATP (upper right panel) in the absence of extracellular Ca^{2+} in EA.hy926 cells treated with either negative control siRNA (Scrambled siRNA, black curves) or siRNA against EMRE and MCU (siEMRE/siMCU, red curves). Statistical analysis of maximum $NO^{\bullet}$ formation in cells stimulated with either 1 μM ATP (lower left panel) representing Scrambled siRNA (white bar, N=3) and siEMRE/siMCU (red bar, N=3); **p=0.0045, with 5 μM ATP (lower middle panel) representing Scrambled siRNA (white bar, N=3) and siEMRE/siMCU (red bar, N=3); **p=0.0087, or with 100 μM ATP (lower right panel) representing Scrambled siRNA (white bar, N=3) and siEMRE/siMCU (red bar, N=3); **p=0.0012.

Europe PMC Funders Author Manuscripts

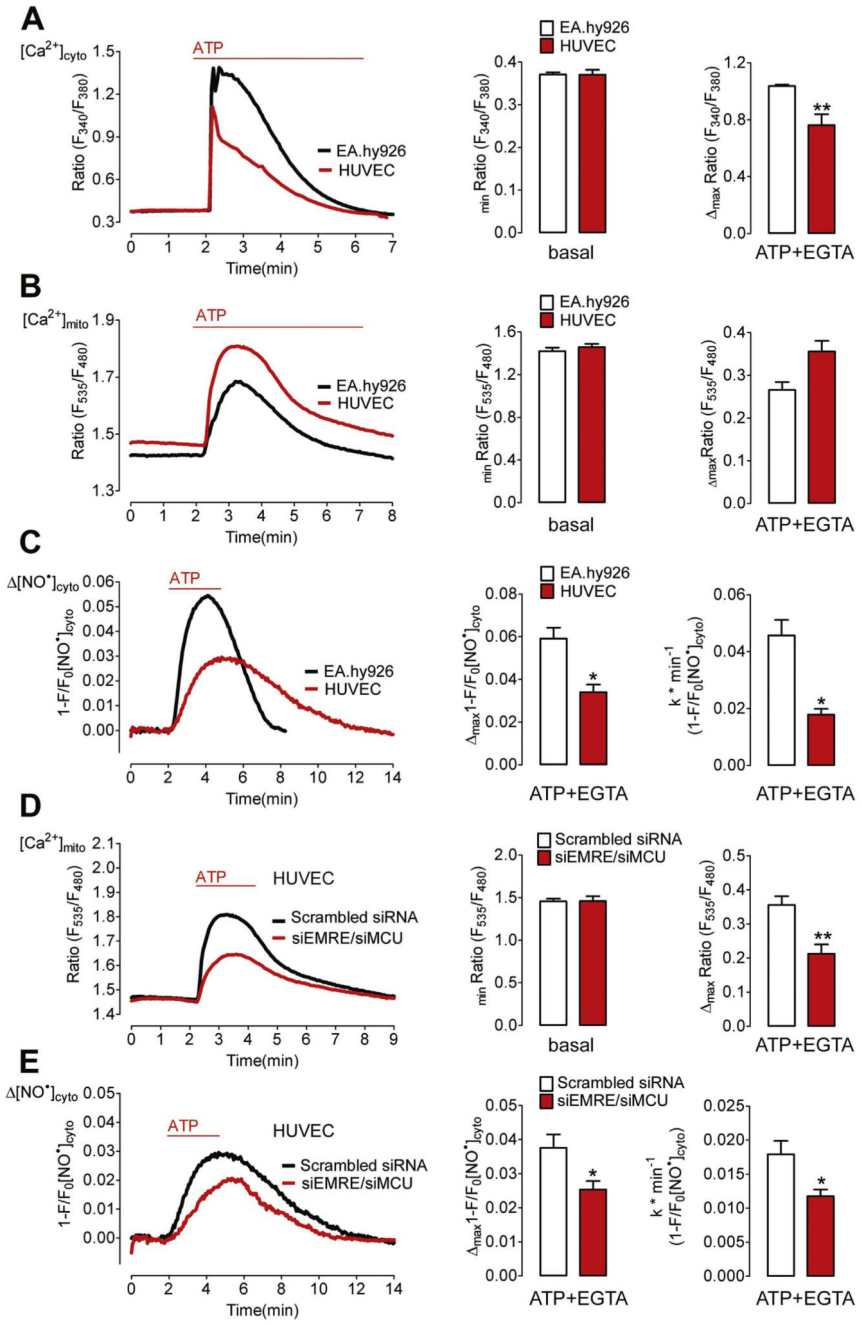

Fig. 3. Knock-down of EMRE/MCU reduces Ca^{2+}-evoked $NO^{\bullet}$ formation in HUVECs.

(A) Cytosolic Ca^{2+} signals in EA.hy926 cells (black curve and white bars) and primary HUVECs (red curve and red bars) in response to 100 μM ATP. $[Ca^{2+}]_{cyto}$ was imaged using fura-2/am loaded cells. Middle bars represent basal fura-2 ratio (F_{340}/F_{380}) values of EA.hy926 cells (white bars, N =6, p=0.9708) and HUVECs (red bars, N =6). Right bars show maximal fura-2 ratio amplitudes in EA.hy926 (white bars, N =6) and HUVEC cells (red bars, N =6). **p=0.005 vs. EA.hy926 cells. (B) Mitochondrial Ca^{2+} signals in EA.hy926 cells (black curve and white bars) and primary HUVECs (red curve and red bars)

in response to 100 μM ATP. $[Ca^{2+}]_{mito}$ was imaged using cells expressing 4mtD3cpV. Middle bars represent basal 4mtD3cpV ratio (F_{535}/F_{480}) values of EA.hy926 cells (white bars, N =3, p=0.4753) and HUVECs (red bars, N =6). Right bars show maximal 4mtD3cpV ratio amplitudes in EA.hy926 (white bars, N =3) and HUVEC cells (red bars, N =6). (C) Cytosolic $NO^{\bullet}$ signals in EA.hy926 cells (black curve and white bars) and primary HUVECs (red curve and red bars) in response to 100 μM ATP. $[NO^{\bullet}]_{cyto}$ was imaged using cells expressing G-geNOp. Middle bars represent maximal fluorescence changes of G-geNOp ($1-F/F_0$) expressed in EA.hy926 cells (white bars, N =10) and HUVECs (red bars, N =8); *p=0.0366 vs EA.hy926. Right bars show maximal slopes of G-geNOp fluorescence changes in response to 100 mM ATP in EA.hy926 (white bars, N =10) and HUVEC cells (red bars, N =8). *p=0.015 vs. EA.hy926 cells. (D) Mitochondrial Ca^{2+} signals in HUVECs under control conditions (Scrambled siRNA, black curve, white bars, N =6) and in cells treated with siRNA against EMRE and MCU (siEMRE/siMCU, red curve, red columns, N =6). Middle bars represent basal 4mtD3cpV ratio values (p=0.1502). Cells were stimulated with 100 μM ATP in the absence of extracellular Ca^{2+}. Right bars show maximal 4mtD3cpV ratio changes upon cell stimulation.**p=0.0032 vs Scrambled siRNA. (E) Cytosolic $NO^{\bullet}$ signals ($[NO^{\bullet}]_{cyto}$) in control HUVECs (Scrambled siRNA, black curve and white bars, N =8) and cells treated with siRNA against EMRE and MCU (siEMRE/siMCU, red curve and bars, N =8) in response to 100 μM ATP in EGTA (1 mM). Middle columns represent mean of maximal ATP-evoked G-geNOp responses; *p=0.0193. Right columns show respective maximal slopes of G-geNOp signals; *p=0.0206.

Europe PMC Funders Author Manuscripts

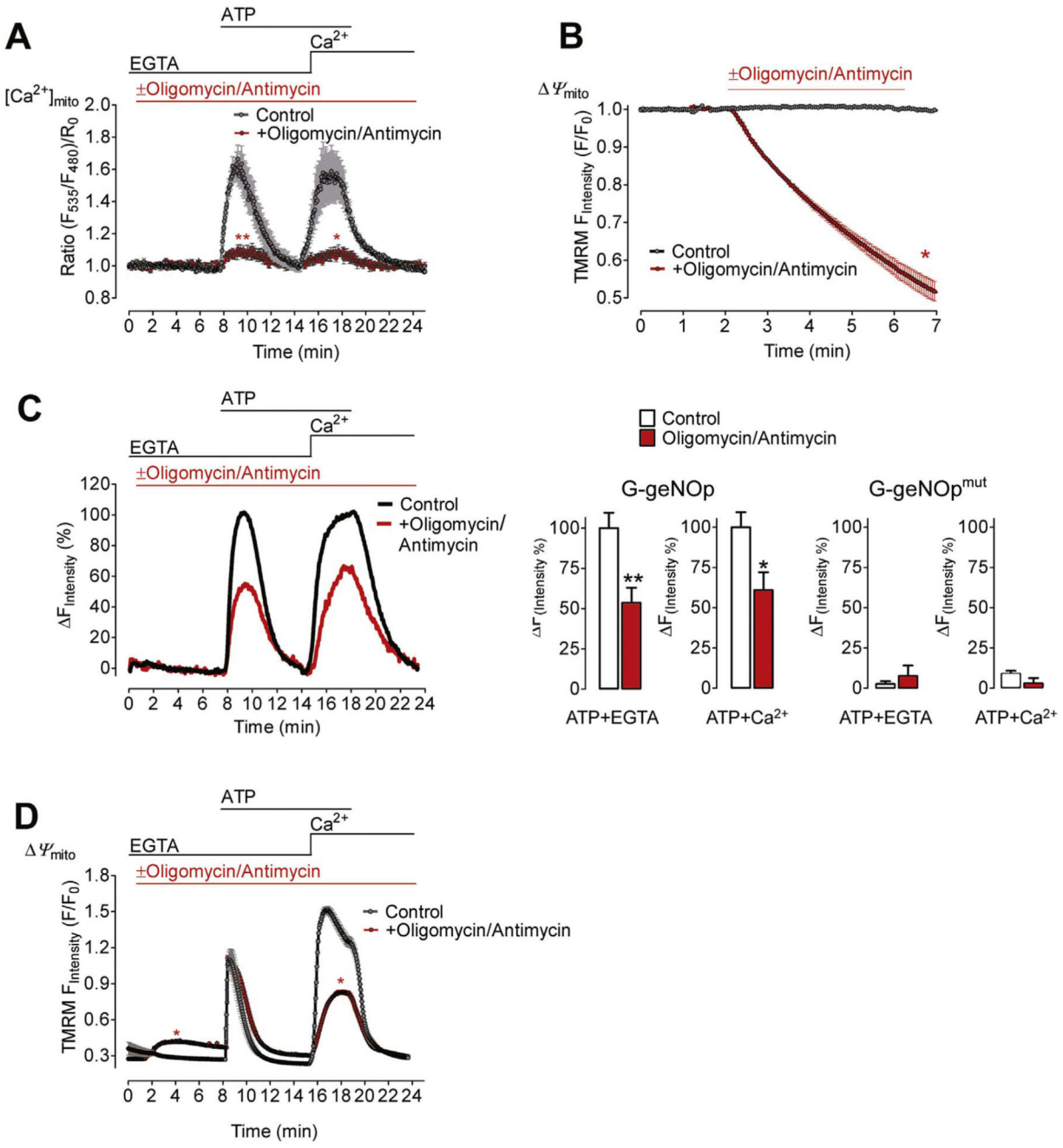

Fig. 4. Cell treatment with oligomycin/antimycin reduces Ca^{2+}-triggered $NO^{\bullet}$ formation.

(A) Average $[Ca^{2+}]_{mito}$ signals ± SEM of EA.hy926 cells expressing 4mtD3cpv under control conditions (black curve N =8) and in the presence of 1 μM oligomycin and 5 μM antimycin (red curve, N =12) in response to 100 μM ATP first in the absence of extracellular Ca^{2+}(1 mM EGTA) and upon addition of Ca^{2+}(2 mM).**p=0.0096 (in EGTA) and *p=0.0159 (in Ca^{2+}) vs. Control. (B) TMRM signals of EA.hy926 cells over time to estimate changes in Ψ_{mito} (mitochondrial membrane potential) under control conditions (black curve N =6) and upon addition of 1 μM oligomycin and 5 μM antimycin (red curve, N

=6). *p=0.0286. (C) $NO^{\bullet}$ signals of EA.hy926 cells over time expressing G-geNOp in the absence (control, black curve, white bars, N =11) or presence of 1 μM oligomycin and 5 μM antimycin (red curve and bars, N =9). Maximal signals under control conditions in response to 100 μM ATP were defined as 100% (middle right bars). **p=0.0074 (in EGTA) and *p=0.0200 (in Ca^{2+}) vs. Control. Right bars represent maximal fluorescence changes of the $NO^{\bullet}$-insensitive G-geNOp^{mut} in control cells (white bars N =6) and in the presence of the mitochondria toxins (red bars, N =6). p=0.8016 (in EGTA) and p=0.1508 (in Ca^{2+}). (D) Fura-2 ratio signals of EA.hy926 cells over time under control conditions (black curve, N =6) and in the presence of 1 μM oligomycin and 5 μM antimycin (red curve, N =6). *p=0.0286 (in EGTA) and *p=0.0283 (in Ca^{2+}) vs. Control.

Europe PMC Funders Author Manuscripts

Europe PMC Funders Author Manuscripts

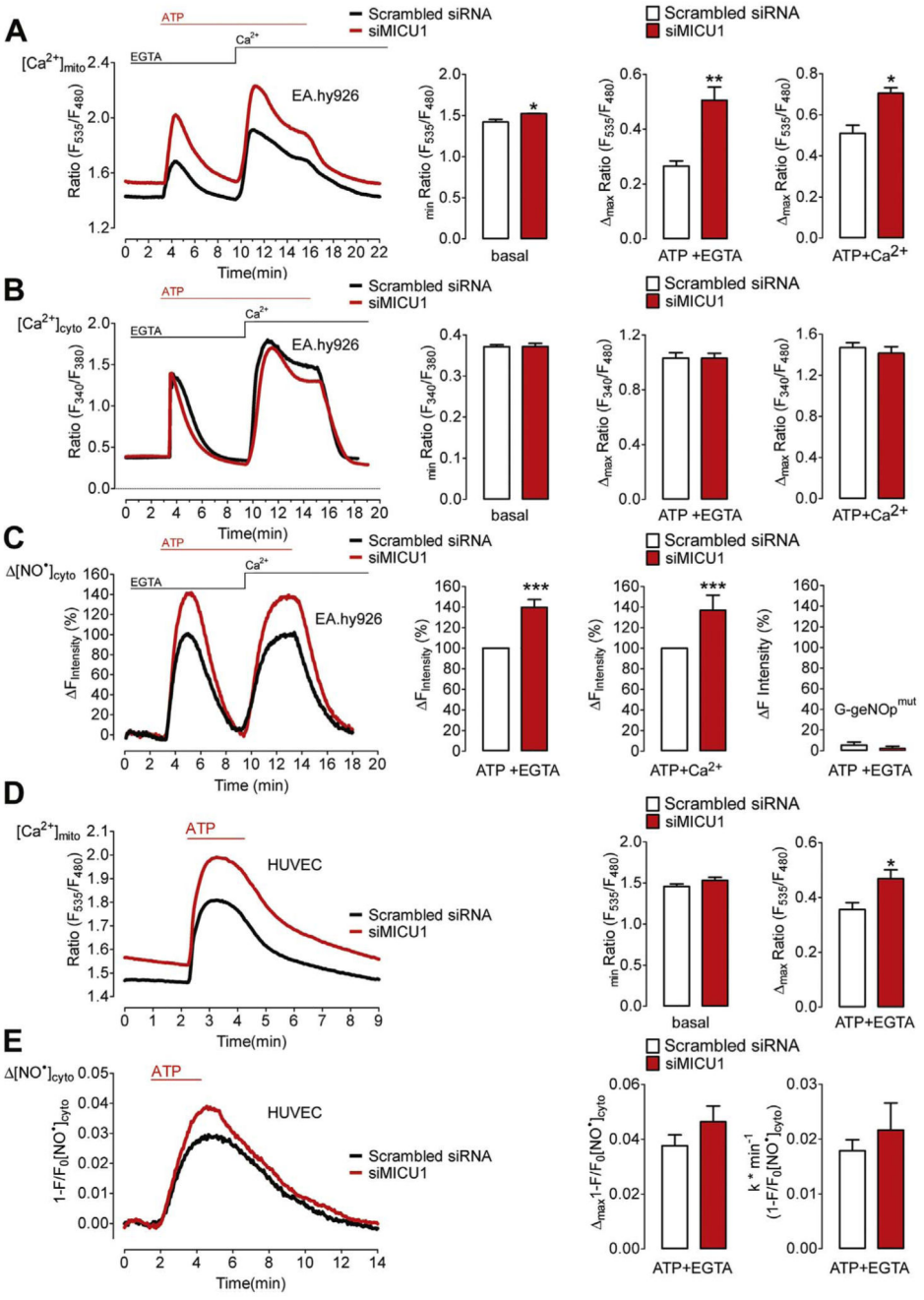

Fig. 5. Silencing of MICU1 increases Ca^{2+}-triggered $NO^{\bullet}$ production in endothelial cells.

(A) Average curves of $[Ca^{2+}]_{mito}$ (left panel) in EA.hy926 cells treated with either scrambled siRNA (black curve and white bars, N=3) or siRNAs against MICU1 (siMICU1, red curve and red bars, N=3) upon stimulation with 100 μM ATP in the absence of extracellular Ca^{2+}(1 mM EGTA) followed by addition of Ca^{2+}(2 mM). Bar graphs showing average basal Ca^{2+} level (basal, *p=0.0356) and Ca^{2+} transients in response to 100 μM ATP in 1 mM EGTA (ATP + EGTA, **p=0.0098) and upon Ca^{2+} addition (ATP + Ca^{2+}, *p=0.0151). (B) Curves representing average of $[Ca^{2+}]_{cyto}$ in control (Scrambled siRNA, black curve, N=6)

versus MICU1 ablated (siMICU1, red curve, N=6) EA.hy926 cells (left panel) stimulated with 100 μM ATP in the absence (1 mM EGTA) and addition of Ca^{2+}(2 mM) as indicated. Respective statistical analyses of basal levels (basal, p=0.9621), maximum cytosolic Ca^{2+} release (ATP + EGTA, p=0.9911) and maximum cytosolic Ca^{2+} entry (ATP + Ca^{2+}, p=0.4977). (C) Representative curve of $[NO^{\bullet}]_{cyto}$ in response to ATP stimulation. Statistical analyses of average $[NO^{\bullet}]_{cyto}$ are shown in bar graphs (right panels). Maximal signals (amplitude) of scrambled siRNA- or siMICU1-treated cells are defined as 100%. Cells were first stimulated with 100 μM ATP in the absence of extracellular Ca^{2+} in control cells (Scrambled siRNA, white column, ATP + EGTA, N =17) and cells reduced of MICU1 (siMICU1, red column, ATP + EGTA, N =16) and upon Ca^{2+}(2 mM) addition (right middle column pair). **p=0.0083 (ATP + EGTA) and **p=0.0079 (ATP+Ca^{2+}) vs Scrambled siRNA. Right columns represent maximal fluorescence changes of G-geNOp^{mut} in response to 100 μM ATP in EGTA (1 mM) in control cells (white column, N =11) and cells treated with siRNA against MICU1 (siMICU1, red column, N =8); p=0.4424 vs Scrambled siRNA. (D) Mitochondrial Ca^{2+} signals in HUVECs under control conditions (Scrambled siRNA, black curve, white bars, N =6) and in cells treated with siRNA against MICU1 (siMICU1, red curve, red columns, N =6). Middle bars represent basal 4mtD3cpV ratio values (p=0.1502). Cells were stimulated with 100 μM ATP in the absence of extracellular Ca^{2+}. Right bars show maximal 4mtD3cpV ratio changes upon cell stimulation.*p=0.0211 vs Scrambled siRNA. (E) Cytosolic $NO^{\bullet}$ signals ($[NO^{\bullet}]_{cyto}$) in control HUVECs (Scrambled siRNA, black curve and white bars, N =8) and cells treated with siRNA against MICU1 (siMICU1, red curve and bars, N =10) in response to 100 μM ATP in EGTA (1 mM). Middle columns represent mean of maximal ATP-evoked G-geNOp responses; p=0.2532. Right columns show respective maximal slopes of G-geNOp signals; p=0.4567.

Europe PMC Funders Author Manuscripts

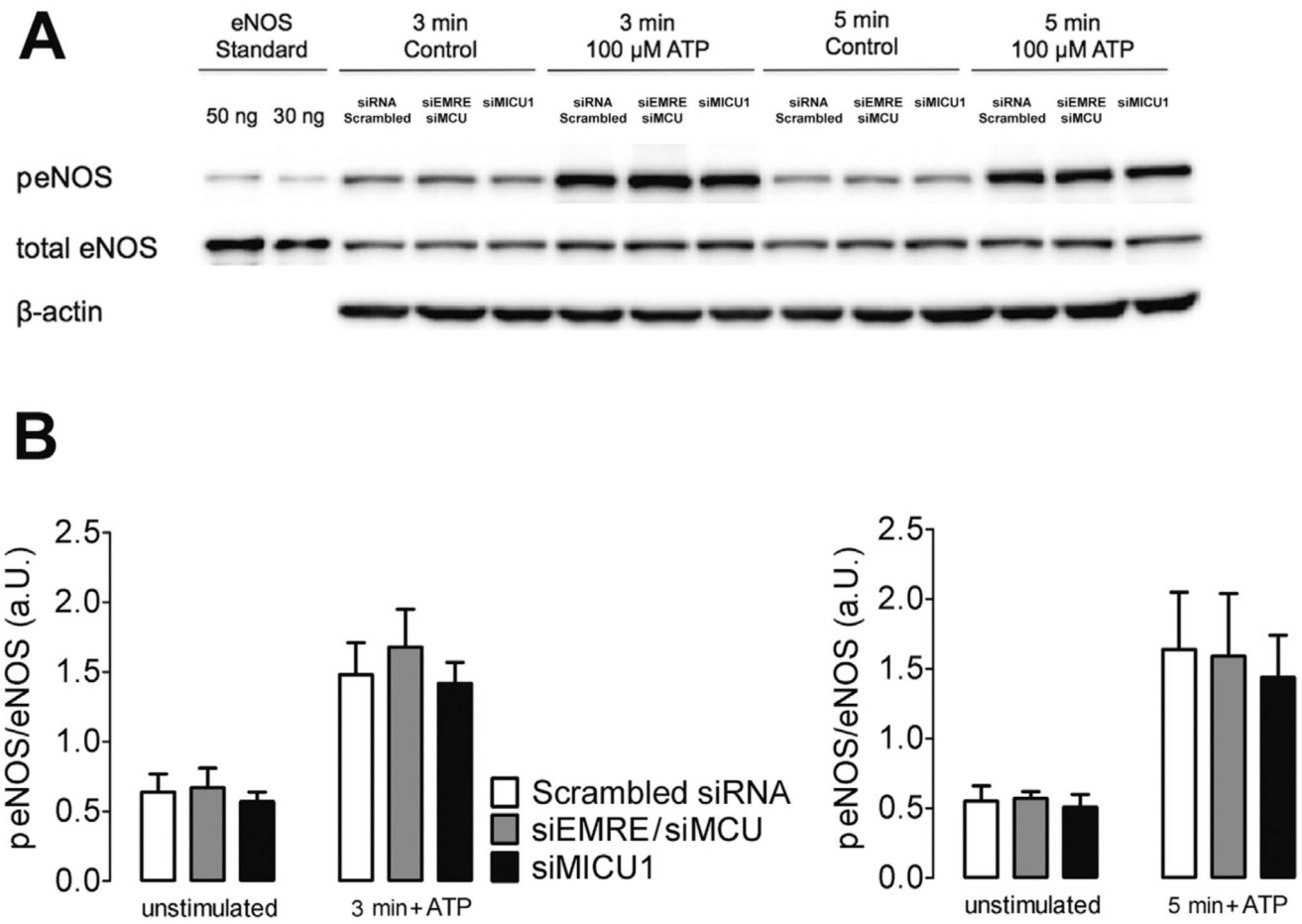

Fig. 6. The expression level and phosphorylation status of eNOS remain unaffected by transient down-regulation of MCU, EMRE and MICU1.

(A) Representative Western blot of total homogenates of transfected EA.hy926 cells (30 μg of protein) showing phosphorylated eNOS (peNOS; 140 kDa), total eNOS (140 kDa) and β-actin (43 kDa) under basal conditions (unstimulated) or stimulated with 100 μM ATP for 3 or 5 min. Purified human eNOS (30 and 50 ng) was used as standard. Bands of control cells (Scrambled siRNA) and cells treated with siRNA against both EMRE and MCU (siEMRE/siMCU) or against MICU1 (siMICU1) are shown. (B) Bars show the ratio of phosphorylated to total eNOS protein in transfected EA.hy926 cells (Scrambled siRNA, siEMRE/siMCU and siMICU1) under basal conditions (unstimulated), after 3 (left panel) and 5 (right panel) minutes of incubation with 100 μM ATP. N =3 for all conditions.

Europe PMC Funders Author Manuscripts

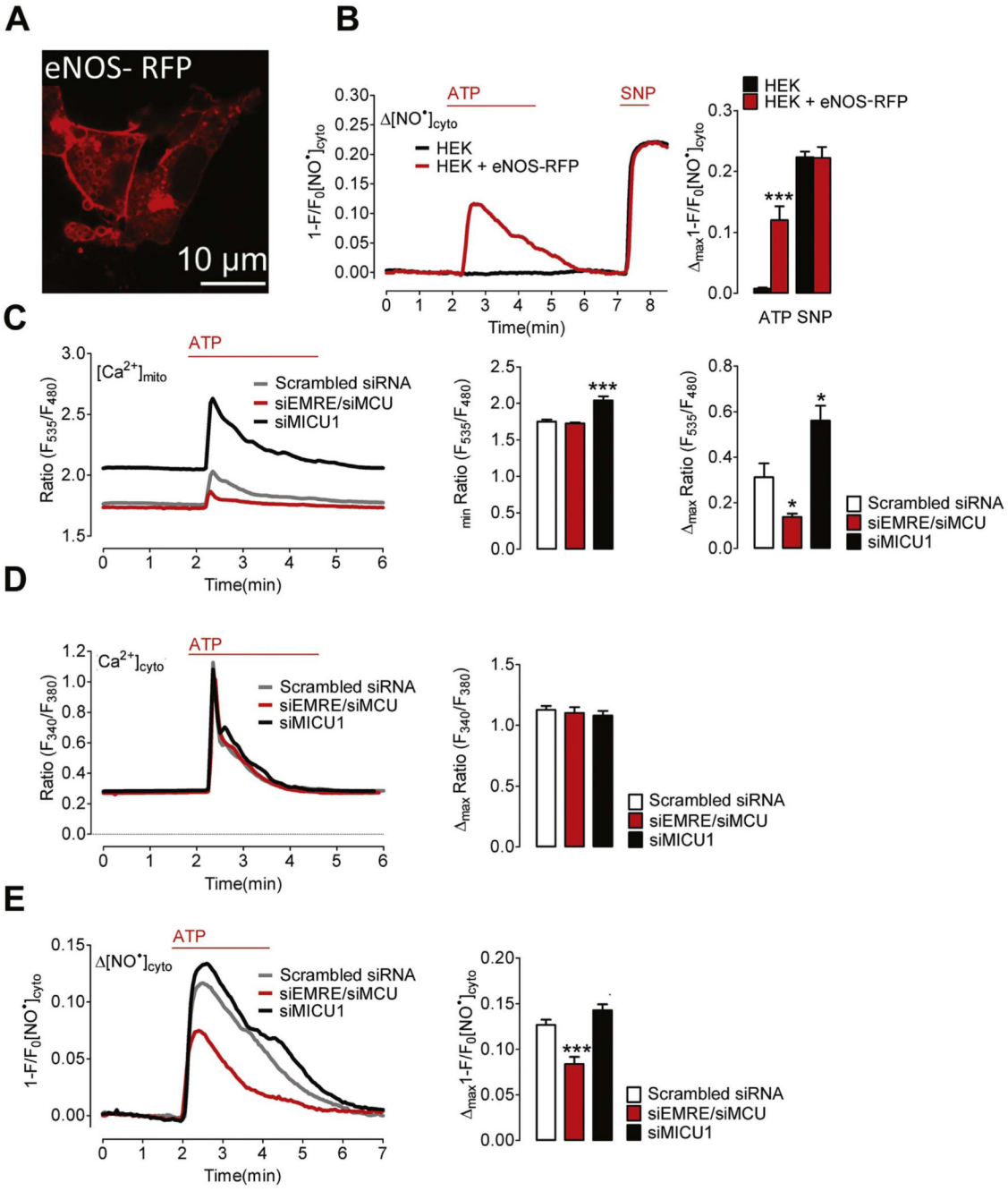

Fig. 7. Mitochondrial Ca^{2+} uptake controls $NO^{\bullet}$ formation in HEK293 cells expressing eNOS-RFP.

(A) Representative image showing HEK293 cells expressing eNOS-RFP. (B) Representative curves of cytosolic $NO^{\bullet}$ signals ($[NO^{\bullet}]_{cyto}$) over time in response to 100 μM ATP and 1 mM SNP in control HEK293 cells (black curve and bars, N =5) and HEK293 cells co-expressing eNOS-RFP (red curve and bars, N =3). Left Bars show maximal changes of G-geNOp fluorescence in response to ATP; ***p=0.0005 vs HEK293. Right bars show maximal G-geNOps signals in response to SNP, p=0.9386. (C) Mitochondrial Ca^{2+} signals in HEK293 cells under control conditions (Scrambled siRNA, grey curve and white columns, N =8), in

cells treated with siRNA against EMRE and MCU (siEMRE/siMCU, red curve and red columns, N =8) or against MICU1 (siMICU1, black curve and columns, N =7). Cells were stimulated with 100 μM ATP in EGTA (1 mM). Left columns represent basal 4mtD3cpV ratio values; p=0.4088 (siEMRE/siMCU) vs Scrambled siRNA; ***p=0.0004 (siMICU1) vs Scrambled siRNA. Right columns show mean values of maximal 4mtD3cpV ratio signals; *p=0.0145 (siEMRE/siMCU) vs Scrambled siRNA; *p=0.0152 (siMICU1) vs Scrambled siRNA. (D) Representative cytosolic Ca^{2+} signals of fura-2/am loaded HEK293 cells treated with scrambled siRNA (Scrambled siRNA, grey curve and white columns, N =3) siRNA against EMRE and MCU (siEMRE/siMCU, red curve and red columns, N =3) or MICU1 (siMICU1, black curve and columns, N =4). Cells were stimulated with 100 μM ATP in EGTA (1 mM). Columns represent mean values of maximal fura-2 ratio signals; p=0.6842 (siEMRE/siMCU) vs Scrambled siRNA; p=0.4253 (siMICU1) vs Scrambled siRNA. (E) Representative cytosolic $NO^{\bullet}$ signals eNOS-RFP expressing HEK293 cells treated with scrambled siRNA (Scrambled siRNA, grey curve and white columns, N =9) siRNA against EMRE and MCU (siEMRE/siMCU, red curve and red columns, N =11) or MICU1 (siMICU1, black curve and columns, N =8). Cells were stimulated with 100 μM ATP in EGTA (1 mM). Columns represent mean values of maximal G-geNOp signals; ***p=0.0005 (siEMRE/siMCU) vs Scrambled siRNA; p=0.0829 (siMICU1) vs Scrambled siRNA.